# $TiCl_4$ Immobilized on a Composite Support $SiO_2$/$MgCl_2$·x(1,4-butanediol)/Poly[styrene-*co*-(acrylic acid)] for Ethylene Polymerization: The Barrier Effect of Poly[styrene-*co*-(acrylic acid)]

**Binbo Jiang, Lijun Du, Fang Wang, Jian Ye, Jingdai Wang, Yongrong Yang**

*State Key Laboratory of Chemical Engineering, Department of Chemical and Biological Engineering, Zhejiang University, Hangzhou 310027, People's Republic of China*

Received 11 July 2011; accepted 29 September 2011
DOI 10.1002/app.36339
Published online 6 January 2012 in Wiley Online Library (wileyonlinelibrary.com).

**ABSTRACT:** By immobilizing titanium-based Ziegler–Natta catalyst on composite support, $SiO_2$/$MgCl_2$·x(1,4-butanediol)/poly[styrene-*co*-(acrylic acid)] ($SiO_2$/$MgCl_2$·xBD/PSA) and $SiO_2$/$MgCl_2$·xBD/PSA/$TiCl_4$ (SMPT) were synthesized for ethylene polymerization. $SiO_2$/$MgCl_2$·xBD/$TiCl_4$ without PSA was also prepared for comparison. The results of energy-dispersive X-ray analysis, SEM, and thermogravimetric analysis demonstrated that SMPT had a unique core-mantle-shell structure. The PSA layer can be considered as a barrier for the mass-transfer of reactants based on the results of self-diffusion measurement by pulsed field gradient NMR and ethylene polymerization. The polyethylene produced by SMPT showed high molecular weight (MW) and broad molecular weight distribution (MWD). The influences of PSA content, hydrogen, and comonomer on the ethylene polymerization behavior were also investigated. The results further demonstrated that the PSA layer in the composite support had different diffusion capabilities to the reactants. The physical properties of the produced polyethylene implied the possibility to control the MW and MWD of polyethylene by the manipulation of PSA layer. The catalyst fragmentation during ethylene polymerization was also affected by the PSA shell due to its barrier effect. © 2012 Wiley Periodicals, Inc. J Appl Polym Sci 125: 1207–1218, 2012

**Key words:** inorganic/organic composite support; barrier; Ziegler–Natta polymerization; polyethylene

## INTRODUCTION

Ziegler–Natta catalysis remains one of the most important and profitable process although more than 50 years have passed since its discovery.[1,2] Olefin polymerization in slurry and gas phase reactors requires the use of solid-supported catalysts.[1–3] The most important characteristics of solid-supported catalysts in olefin polymerization, for example, fragmentation phenomena, activity profile, particle growth, and final polymer morphology and some other properties, are directly affected by the nature of supports.[4,5]

Beside inorganic supports, such as $MgCl_2$,[6,7] silica,[8,9] mixture of $MgCl_2$ and silica,[10,11] and so on, polymer materials have also been applied as supports for Ziegler–Natta catalysts.[12,13] Polymer supports are able to eliminate some side effects of inorganic supports, such as reduction in ash content.[14,15] Furthermore, the chemical environment and structure of polymer-supported catalysts can be manipulated by different functional groups and back bones of the polymer supports.[16,17] This provides an opportunity to directly investigate how the chemical environments of the polymer-supported catalysts influence the olefin polymerization.[12,17,18]

Because of the improved performance, tailored high-density polyethylene with very broad or bimodal molecular weight distribution (MWD) received much attention. However, the classical heterogeneous Ziegler–Natta catalysts usually produce polyethylene with medium MWD. A cascade reactor is usually used for producing such tailored polyethylene.[1,19,20] A large investment is required to build up and operate such a cascade reactor. So, production of tailored high-density polyethylene in one reactor is attractive. This may be realized by a tailor-designed catalyst. Usually, the polyethylene

*Correspondence to:* B. Jiang (Jiangbb@zju.edu.cn).
Contract grant sponsor: National Natural Science Foundation of China; contract grant number: 21076180.
Contract grant sponsor: Fundamental Research Funds for the Central Universities; contract grant number: 2009QNA4028.
Contract grant sponsor: Project Based Personal Exchange Program (PPP) from China Scholarship Council; contract grant number: 20083070.

produced by heterogeneous catalysts has broader MWD than that by homogeneous catalysts.[21] The chemical theory and the diffusion theory are the main theories for discussion of this. Based on the chemical theory, the heterogeneous catalysts have two or more different active species producing polymers with two or more different mean molecular weight (MW) under the same polymerization conditions. The MWD is then associated to the number of active species and to the difference between these active species. Multiple active sites positioning on one catalyst particle is often realized by synthesis of hybrid or mixed catalyst. However, the hybrid or mixed catalysts are hard to be kinetically and chemically compatible on the same support. According to the diffusion theory, the barrier to the transfer of monomer or heat results in distributions of polymerization conditions in a growing polymer particle and thus in distributions of chain lengths. The more important the diffusion barrier, the broader the expected MWD will be. However, the researchers have not paid enough attention on the diffusion theory. Recently, considerable effort has been devoted to immobilize catalysts on inorganic/polymer composite supports. As the performance of supported catalysts strongly depend on the physical and chemical properties of support,[8,22] different types of active sites could be created by supporting catalysts on inorganic/polymer composite particles with multiple chemical environments. In general case, polymer-supported Ziegler–Natta catalysts[23–26] can produce polyethylene with different MW compared with the inorganic-supported Ziegler–Natta catalysts.[24] Kaur et al.[25] immobilized $TiCl_4$ on mixed support of $MgCl_2$·xEB/poly(methyl acrylate-*co*-1-octene) and the produced polyethylene showed broad MWD. Guo et al.[23] and Liu et al.[26] synthesized a kind of $SiO_2$/polymer microspheres with core-shell structure to support metallocene catalysts for ethylene polymerization, respectively. Although the polymer was considered as a part of the hybrid support, the diffusion theory for interpretation of the very broad MWD of polymer was not discussed in the articles.

We have developed an improved phase inversion method to prepare polymer-coated $SiO_2$ microspheres.[27] These microspheres have been successfully used to support Ziegler–Natta or hybrid Ziegler–Natta/metallocene catalysts for production of polyethylene with broad or bimodal MWD.[28,29] Besides the role as the hybrid support, our results implied that the polymer affected the mass transfer of different reactants. This difference was also considered to be critical for the production of polyethylene with broad MWD. In the present work, we synthesized a titanium-based Ziegler–Natta catalyst immobilizing on an inorganic/polymer composite support with a unique core-mantle-shell structure for ethylene polymerization. On the basis of the previous studies, we focused our investigation on effects of the polymer shell. Large amount of hydrocarbon solvent is needed to precipitate $MgCl_2$ from an alcoholic solution at high temperature in industrial applications.[3,5,30] However, we found that a small amount of BD was rather effective to precipitate $MgCl_2$ from a tetrahydrofuran (THF) solution.[31] $SiO_2/MgCl_2$·xBD were generated when BD was added into the $MgCl_2$/THF solution with suspended $SiO_2$ particles. By coating poly[styrene-*co*-(acrylic acid)] (PSA) on $SiO_2/MgCl_2$·xBD, composite support $SiO_2/MgCl_2$·xBD/PSA was synthesized and used as support for titanium-based Ziegler–Natta catalysts. The supports and catalysts were then characterized by several techniques, including SEM, energy dispersive X-ray (EDX) analysis, thermogravimetric analysis (TGA), elemental analysis, and pulsed field gradient NMR. Ethylene homopolymerization and copolymerization were carried out to evaluate the synthesized catalysts.

## EXPERIMENTAL

### Materials

All chemicals were handled either in a glove box or under inert nitrogen atmosphere using standard Schlenk techniques. High-purity nitrogen, polymerization-grade ethylene, and hydrogen were supplied by Sinopec Shanghai Corporation and purified by sequentially passing them through copper catalyst column and alumina column. Solvents (*n*-heptane, *n*-hexane, and THF) were dried over 4-Å molecular sieves for at least 10 days and then purified by solvent purification system of Innovative Technology. Silica 2485 ($SiO_2$) from W. R. Grace was activated at 600°C for 4 h with nitrogen flow. Titanium (IV) chloride ($TiCl_4$, $\geq$98.0% wt) was used as received from Sinopharm Chemical Reagent. Anhydrous magnesium chloride was kindly donated by Sinopec Tianjin Corporation. 1,4-Butanediol [$HOCH_2CH_2CH_2CH_2OH$, BD] from Sinopharm Chemical Reagent were dried by 4-Å molecular sieves for 10 days before use. Triethylaluminium (TEA) was purchased from Aldrich. Poly(styrene-*co*-acrylic acid) (PSA) provided by Changchun Institute of Applied Chemistry was produced by free radical polymerization method. PSA was dried at 70°C under nitrogen flow for 24 h before use. The average MW of PSA was 19,225 and the MWD is 2.4, with about 3.5 mmol —COOH/g PSA.

### Preparation of supports and catalysts

Synthesis of $SiO_2/MgCl_2$·xBD

$SiO_2$ (3.00 g) stirred together with BD (0.75 mL) in THF (20 mL) at 55 °C for 1 h. $SiO_2/x$BD was prepared by drying the resultant slurry under vacuum

for 2 h would leave on silica as it cannot be removed by the vacuum at this low temperature due to its high boiled temperature (228°C). $MgCl_2$ (0.60 g) placed in another Schlenk flask was stirred in THF (25 mL) until complete dissolution. The previously prepared $SiO_2/x$BD was then added into the $MgCl_2$/THF solution. Because of the strong coordination between $MgCl_2$ and BD,[31] $MgCl_2$ immediately precipitated on the surface of $SiO_2$. The stirring was continued for another 1 h.

### Synthesis of $SiO_2/MgCl_2{\cdot}$xBD/$TiCl_4$

The residual white solids present in $SiO_2/MgCl_2{\cdot}$**x**BD/THF mixture were separated, washed with dry *n*-hexane (3 × 40 mL), and dried under vacuum for 2 h. $SiO_2/MgCl_2{\cdot}$xBD/$TiCl_4$ (SMT) was synthesized by supporting $TiCl_4$ (2.68 mL) on the resultant $SiO_2/MgCl_2{\cdot}$**x**BD, which were suspended in *n*-hexane (30 mL) at 55°C. The color of the mixture instantaneously became fresh yellow with the addition of $TiCl_4$. After the addition of $TiCl_4$, the reaction mixture was stirred for another 2 h under nitrogen. The residual solids were separated, washed with dry *n*-hexane (5 × 40 mL) to completely remove excess $TiCl_4$, and dried under vacuum for 3 h.

### Synthesis of $SiO_2/MgCl_2{\cdot}$xBD/PSA/$TiCl_4$

PSA/THF solution (0.1 g/mL) was prepared by dissolving PSA (10.0 g) in THF (100 mL) at ambient temperature. Calculated amount of PSA/THF solution was injected into the previous prepared $SiO_2/MgCl_2{\cdot}$**x**BD/THF mixture and stirred for 30 min at 0°C. *N*-hexane (100 mL) was then introduced into the mixture through vapor phase.[27] The PSA slowly separated from THF and precipitated on $SiO_2/MgCl_2{\cdot}$**x**BD. The resulting slurry was decanted, washed by *n*-hexane (3 × 40 mL), and dried under vacuum for 2 h. Then *n*-hexane (40 mL) were added into the generated solids and stirred together at 0°C. Slowly, via syringe, $TiCl_4$ (2.68 mL) was introduced to the slurry and kept at 0°C for 1 h. The temperature was increased to 40°C in the flask and maintained for 1 h. The reaction was continued for another 2 h at 60°C. After removal of the extra $TiCl_4$, the solid catalyst ($SiO_2/MgCl_2{\cdot}$xBD/PSA/$TiCl_4$, SMPT) was washed by *n*-hexane (5 × 40 mL) at 60°C and dried under vacuum for 3 h.

### Ethylene polymerization

Slurry ethylene homopolymerization and copolymerization were carried out in a 1-L Büchi stainless steel autoclave reactor, equipped with a mechanical stirrer, a mass flow meter, and a temperature control unit consisting of cooling water and an electric heater. Prior to each reaction, the reactor was heated above 85°C under vacuum for more than 2 h and repeatedly pressurized with nitrogen, purged, and evacuated (<10 mbar). Then, the reactor temperature was decreased to 75°C. *n*-Heptane (350 mL; and required amount of 1-hexene) was injected into the reactor. The catalyst was introduced into the reactor under nitrogen purging after injection of appropriate TEA as cocatalyst. The prescribed amount of hydrogen was introduced into the reactor as judged by the increase of pressure in the reactor. The polymerization then took place under a continuous ethylene flow to meet the desired pressure. The polymerization rates were taken to be equal to the rate of the ethylene feed required to maintain a constant reactor pressure. At the end of the polymerizations, the reactor was rapidly vented, and the synthesized polymer was precipitated and washed with acidified (2 wt % hydrochloric acid) ethanol, filtered, and dried at 50°C under vacuum for 12 h.

## Characterization

### Characterization of supports

The surface morphology of supports was observed using field emission scanning electron microscope (FESEM, Hitachi S-4700). EDX analysis was performed on an EDAX system attached to the same FESEM apparatus. Samples were fixed on carbon tape on a stub, followed by platinum sputtering. Fourier transform infrared (FTIR) spectrometry measurements were carried out on a Nicolet 5700 spectrometer. Dry microspheres were completely mixed with analytical grade KBr and pressed into a form of tablet, and the spectrum was then recorded.

$^1H$ diffusion and relaxation measurements of *n*-hexane in $SiO_2$ and PSA-coated $SiO_2$ particles were performed on a 300-MHz NMR spectrometer (Bruker Avance) equipped with a field gradient system (DIFF 30, Bruker) providing a maximum gradient strength of 1200 G/cm. *n*-Hexane was chosen as a test substance to determine the geometric restrictions to self-diffusion, because this experiment required a liquid phase to be conducted with sufficient accuracy. The diffusion results of *n*-hexane are representative for the reactants in the polymerization reaction. It is well known that for pore spaces well exceeding the molecular size, the self-diffusion coefficient of the adsorbed species is reduced in comparison to its bulk value by a factor that is dominated by a combination of porosity and connectivity of the pore space, that is, purely geometric factors, and only weakly dependent on the type of adsorbant itself. All measurements were carried out at room temperature (20°C). The spin lattice relaxation time ($T_1$) was measured by inversion recovery

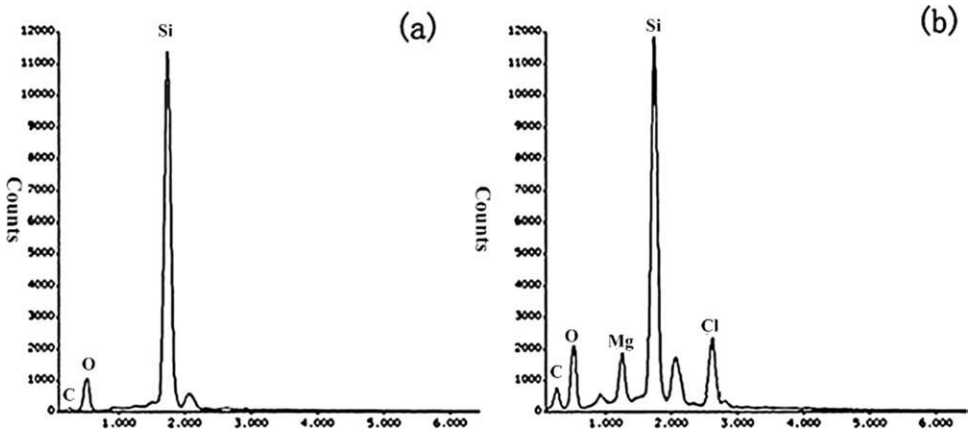


**Figure 1** EDX spectra of (a) $SiO_2$ particle and (b) $SiO_2/MgCl_2{\cdot}$**x**BD particle.

experiments [π-τ-π/2-acquisition]. The pulsed field gradient method was applied to measure the self-diffusion of the *n*-hexane in porous particles. A stimulated echo sequence [π/2-τ-π/2-*T*-π/2-τ-echo] was used in combination with two gradient pulses. Value of δ was typically kept to 1 ms and Δ was 50 ms. Acquisition of each proton spectrum using the pulsed field gradient NMR sequences required 32 scans. The principle for the calculation of diffusion coefficient of *n*-hexane is provided by the literatures.[32,33]

### Characterization of catalysts

The prepared catalysts were also subjected to TGA using Mettler Toledo SDTA851 system. Samples of <10 mg were heated from 25 to 600°C at a heating rate of 10°C/min in nitrogen atmosphere and the corresponding weight loss was recorded. The magnesium content was determined by a titration method using the chelating agent, ethylenediamine tetraacetic acid. The titanium content of the catalysts was determined by ultraviolet spectroscopy (UV). UV measurements were carried out in 10-mm quartz glass cells on Unico UV-2102PC spectrophotometer. The intensity of a peak at 410 nm was used to quantify the titanium content.

### Characterization of polyethylene

The catalyst activity was calculated as the mass of resulting polymer divided by the grams of metal per minute. The melting temperature ($T_m$) of the produced polyethylene was characterized by differential scanning calorimetry (DSC; Perkin-Elmer 7). The nascent polyethylene was heated to 160°C (10°C/min), held at 160°C for 1min, then cooled to 50°C (10°C/min), and held at 50°C for 1 min. Finally, the polyethylene was heated to 160°C (10°C/min), again. The reported melting points were determined based on the peak values of the second heating curves. MW and MWD of the produced polyethylene were measured by gel permeation chromatography (GPC). The PL-220 GPC assay was done at 150°C with 1,2,4-trichlorobenzene as solvent. The universal calibration curve, obtained from narrow MWD polystyrene standards, was used to quantify the results. Melt flow index (MFI) was determined in a fusion index instrument (CEAST, Italy) at 190°C, using a 21.6 kg charge. SEM (Hitachi S-4700) was used to investigate the morphology of the polyethylene particles.

## RESULTS AND DISCUSSION

### Characterization of support

#### EDX results

Single-particle SEM-EDX analysis was performed to investigate the magnesium distribution on the $SiO_2/MgCl_2{\cdot}$**x**BD grain. Figure 1 shows the EDX spectrum collected from a typical $SiO_2$ particle compared with that from $SiO_2/MgCl_2{\cdot}$**x**BD particle. The main elements in $SiO_2$ are Si and O. The trace carbon is from the carbon film itself. The presence of Mg and Cl with more content of O and C are found in $SiO_2/MgCl_2{\cdot}$**x**BD, indicating that $MgCl_2{\cdot}$xBD adduct has successfully precipitated on $SiO_2$. The distinctive signal between Si and Cl is from Pt, which was coated on the samples before measurement to enhace the conductivity. Because of the measurement principle and the difference of the probe depth inside the sample, these results are not quantitative.[34]

#### The effect of PSA on the morphology of composite supports

For a better understanding of the support's morphology, SEM microphotographs were taken at different synthesis stages. All particles presented in Figure 2 are found to be spherical shaped without sharp edges. The surface of original $SiO_2$ was smooth. No obvious variation was observed on the

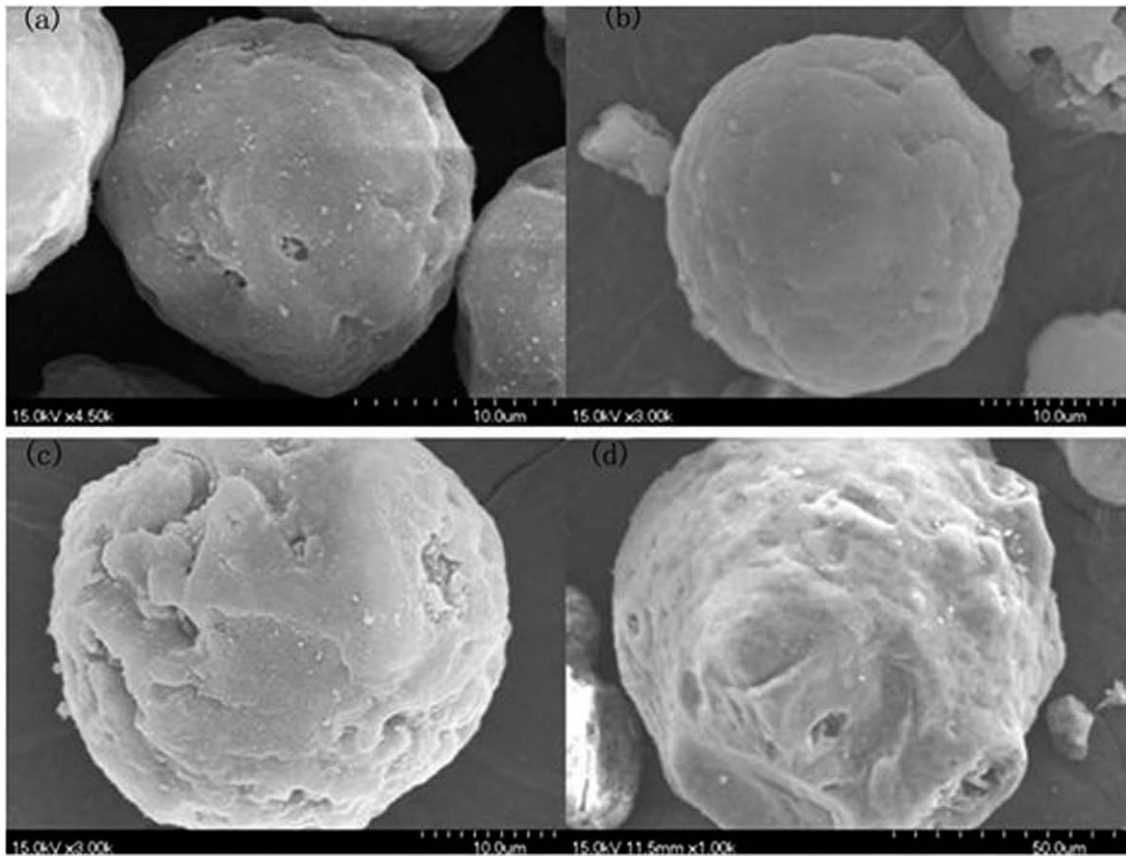


**Figure 2** SEM photographs of supports and catalysts (a) $SiO_2$; (b) $SiO_2$/xBD; (c) $SiO_2/MgCl_2{\cdot}x$BD; (d) $SiO_2/MgCl_2{\cdot}x$BD/PSA.

surface of $SiO_2$ after the treatment with 1,4-(butanediol). As shown in Figure 2(c), a loose and rough shell was created when $MgCl_2{\cdot}x$BD adduct precipitated on the surface of $SiO_2$. Meanwhile, the particle size increased obviously. This confirms that a layer of $MgCl_2{\cdot}x$BD is formed on the surface of $SiO_2$. Smoother surface with larger particle size in Figure 2(d) was observed after PSA coating on $SiO_2/MgCl_2{\cdot}x$BD. The variations in the surface morphology and particle size of the supports imply that the final composite support $SiO_2/MgCl_2{\cdot}x$BD/PSA may have a structure similar to core-mantle-shell structure. $SiO_2$, $MgCl_2{\cdot}x$BD, and PSA correspond to the core, mantle, and shell, respectively.

### Diffusion of n-hexane in the polymer-coated $SiO_2$ and $SiO_2$

Diffusion of *n*-hexane in $SiO_2$ and PSA-coated $SiO_2$ were detected by pulsed field gradient NMR. Pulsed field gradient NMR is a powerful method for the measurement of liquid diffusion in porous media[32,35,36] and has been applied in the characterizations of inorganic/organic core-shell particles.[37,38] As listed in Table I, two diffusion coefficients are calculated according to the signal from pulsed field gradient NMR. The larger diffusion coefficient ($D_1$) is attributed to the diffusion in the part of intraparticles, and the smaller diffusion coefficient ($D_2$) is associated with the diffusion in the part of interparticles. The diffusion coefficient of *n*-hexane in PSA-coated $SiO_2$ particles, either $D_1$ or $D_2$, is smaller than that in $SiO_2$ particles. This indicates that the PSA layer acts as a barrier to the diffusion of *n*-hexane. The volume reduction in the intraparticle space due to the swelling of PSA[39] in *n*-hexane is another reason for the smaller $D_1$. The significant reduction of both the interparticle and intraparticle diffusion coefficients found for *n*-hexane are representative for the corresponding values for the reactants of the polymerization reaction. Meanwhile, the spin-lattice relaxation time ($T_1$) of *n*-hexane in $SiO_2$ and PSA-coated $SiO_2$ particles is 2.233 and 1.799 s, respectively. This result confirms that the mobility of

**TABLE 1**
**Diffusion Coefficient of *n*-Hexane in $SiO_2$ and PSA-Coated $SiO_2$ Particles**

| Sample | $D_1$ ($\times 10^{-9}$ m$^2$/s) | $D_2$ ($\times 10^{-9}$ m$^2$/s) |
|---|---|---|
| $SiO_2$ | 3.22 | 0.203 |
| PSA-coated $SiO_2$ | 1.45 | 0.145 |

**TABLE II**
**The Composition of Different Catalysts**

| Catalyst | SMT | SMPT-1 | SMPT-2 |
|---|---|---|---|
| $SiO_2/MgCl_2/PSA$[a] | 1 : 0.33 : 0 | 1 : 0.33 : 0.3 | 1 : 0.33 : 0.5 |
| Mg (wt %) | 5.76 | 3.44 | 2.78 |
| Ti (wt %) | 13.20 | 3.73 | 4.10 |

[a] The mass ratio of $SiO_2$, $MgCl_2$, and PSA when the catalysts were prepared.

*n*-hexane is more limited in PSA-coated $SiO_2$ particles because restricted molecular mobility also leads to a shortening of the relaxation times, which are related to molecular rotation. A more thorough discussion of the diffusion and relaxation results obtained by NMR will be discussed in a forthcoming paper.

## Characterization of catalysts

### Effect of PSA content on chemical composition of the supported catalysts

The compositions of the supported catalysts are listed in Table II. The weight ratio of $PSA/SiO_2$ was 0, 0.3, and 0.5 in SMT, SMPT-1, and SMPT-2, respectively. The magnesium content of SMT was 5.76%. Because of the addition of PSA, the magnesium content decreased to 3.44% in SMPT-1 and 2.78% in SMPT-2. The titanium content in SMT was as high as 13.20%. This is interpreted by the strong coordination between hydroxyl groups and $TiCl_4$. Hydroxyl groups in 1,4-butanediol can coordinate with a large amount of $TiCl_4$, resulting in high titanium content in SMT. However, the titanium content in SMPT-1 and SMPT-2 was sharply decreased to 3.73 and 4.10%, respectively. The barrier effect of PSA shell is considered to be the main reason for the huge reduction of titanium content. The diffusion of $TiCl_4$ is limited by the PSA layer in synthesis of SMPT. Thus, lower titanium content is detected in SMPT-1 and SMPT-2. At the same time, $TiCl_4$ can be anchored to the —COOH groups in PSA. Thus, the titanium content in SMPT-2 is a slightly higher than in SMPT-1 due to the more PSA content in SMPT-2.

### Results of FTIR spectroscopy

The FTIR spectra in Figure 3 provide the information of reactions between $TiCl_4$ and the composite support.[27,31] The strength of the peak at 1105 $cm^{-1}$ (the asymmetrical stretching of Si—O—Si bond) and 472 $cm^{-1}$ (the bending vibration of Si—O bond) obviously reduced in three catalysts, indicating that $SiO_2$ is in the inner part of catalysts and with no reaction with $TiCl_4$. The typical PSA absorption-bands was at 758 and 698 $cm^{-1}$, which correspond to the phenyl C—H out-of-plane bending and benzene out-of-plane ring bending, respectively [Fig. 3(a)]. However, these two absorption bands shifted to 700 and 606 $cm^{-1}$ both in SMPT-1 [Fig. 3(d)] and SMPT-2 [Fig. 3(f)]. This indicates that $TiCl_4$ has reacted with —COOH in PSA. Further, the signal at 1493 and 1452 $cm^{-1}$ in SMPT-1 and SMPT-2 was much weaker than in PSA. This is because the stretching vibration of C=C in PSA was seriously hindered due to the reaction with $TiCl_4$. Distinctive absorption band at 1632 $cm^{-1}$ is found in all the three catalysts. This signal should be resulted by the reaction between $MgCl_2 \cdot x$BD and $TiCl_4$.

### Effect of PSA on the thermal decomposition of catalysts

TGA was carried out to evaluate the thermal decomposition of the catalysts. The weight loss curves and the corresponding differential curves of PSA, SMT, and SMPT-1 are displayed in Figure 4. A comparison of each differential curve indicates that the thermal decomposition of SMPT-1 [Fig. 4(c)] is similar to the combination of SMT [Fig. 4(a)] and PSA [Fig. 4(b)]. However, the peak temperature associated with decomposition of SMPT-1 was shifted to higher value. Peaks at 83 and 163°C in SMT were moved to 108 and 231°C in SMPT-1, respectively. The width of the two peaks in the curve of SMPT-1 is larger than that of SMT. This indicates that the heat transfer in SMPT-1 is reduced compared with SMT. The decomposition temperature of PSA was increased to 416°C from 400°C after the immobilization of $TiCl_4$. This implies that the thermal stability of PSA is enforced owing to its chemical reaction with $TiCl_4$.

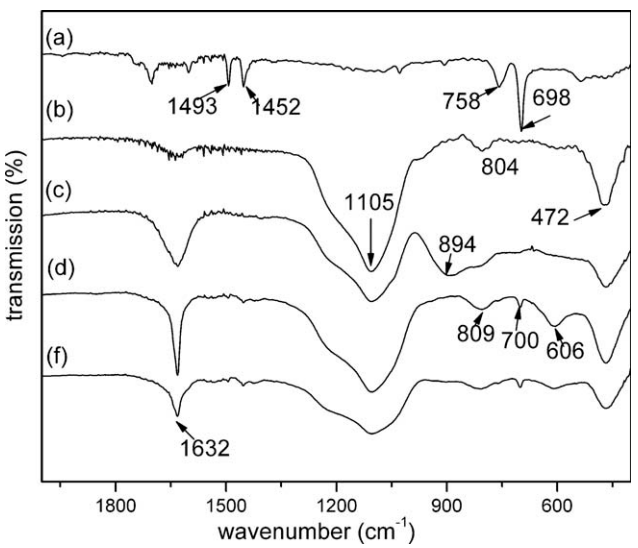


**Figure 3** Comparison of FTIR spectra of supported $TiCl_4$ catalysts with neat supports. (a) PSA; (b) $SiO_2$; (c) SMT; (d) SMPT-1; (f) SMPT-2.

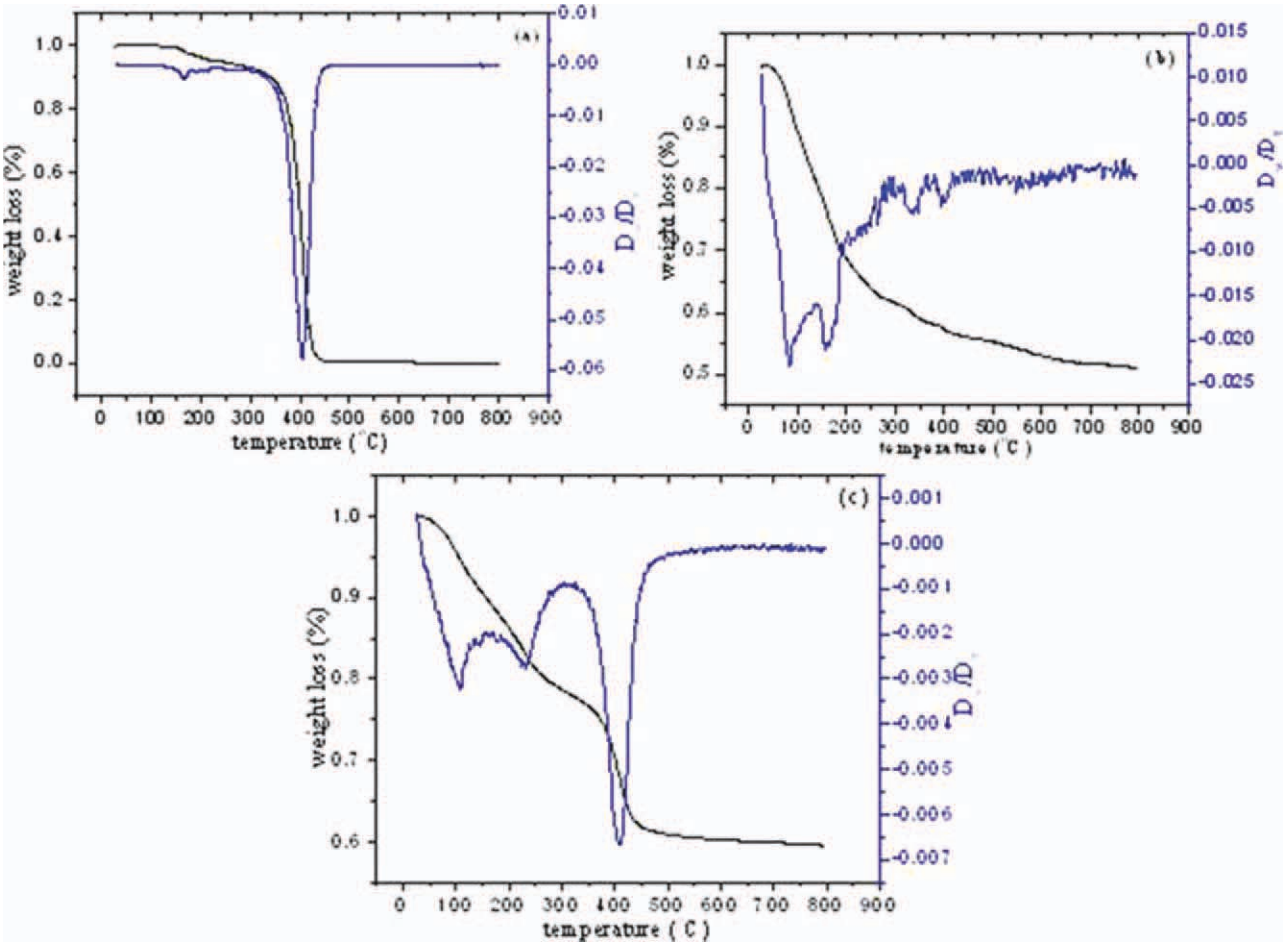


**Figure 4** The weight loss and the corresponding differential curves of (a) PSA, (b) SMT, and (c) SMPT-1. [Color figure can be viewed in the online issue, which is available at wileyonlinelibrary.com.]

## Ethylene homopolymerization and copolymerization

Slurry ethylene polymerizations were carried out to evaluate the supported catalysts. The polymerizations were conducted with Al/Ti molar ratio of 100, at 75°C. The composition of reactants, activity, and other physical properties of the produced polyethylene are listed in Table III. The results are discussed in the following sections.

## Effect of PSA content on activity profiles and properties of the produced polyethylene

The activity profiles are given in Figure 5, indicating that the PSA content strongly affects the catalysts performance. Note that the initial decrease on the curves actually corresponds to the pressurization of the polymerization reactor and should not be interpreted as decay in catalytic activity. Overall, the

**TABLE III**
**The Ethylene Homopolymerization and Copolymerization Results**

| Run | Catalyst | $H_2/C_2H_4$ (mol %) | $C_6H_{12}$ (mol/L) | Activity (g PE/g Ti·h) | Bulk density (g/cm$^3$) | Melting point (°C) | $M_w$ (g/mol) | $M_w/M_n$ | MFI (21.6 kg) |
|---|---|---|---|---|---|---|---|---|---|
| 0 | SMT | 0.5/8.0 | 0 | 9018 | 0.176 | - | 767000 | 3.4 | / |
| 1 | SMPT-1 | 0 | 0 | 54292 | 0.316 | 136.94 | 741600 | 11.6 | / |
| 2 | SMPT-1 | 0.5/8.0 | 0 | 39993 | 0.325 | 132.70 | 491500 | 8.0 | 0.18 |
| 3 | SMPT-1 | 1.0/7.0 | 0 | 32172 | 0.329 | 131.90 | 356300 | 8.0 | 0.55 |
| 4 | SMPT-1 | 4.0/2.8 | 0 | 9717 | - | - | 237500 | 6.8 | - |
| 5 | SMPT-1 | 0 | 0.109 | 58005 | 0.296 | 137.15 | 667400 | 4.7 | / |
| 6 | SMPT-1 | 0 | 0.218 | 30936 | 0.245 | 135.74 | 527200 | 4.1 | 0.03 |
| 7 | SMPT-2 | 0.5/8.0 | 0 | 25797 | 0.309 | - | 483000 | 5.0 | 0.25 |

-, not detected; /, undetectable.

The total pressure was 9.0 bar (ethylene, nitrogen and hydrogen). The polymerization temperature was 75°C. Al/Ti molar ratio was 100.

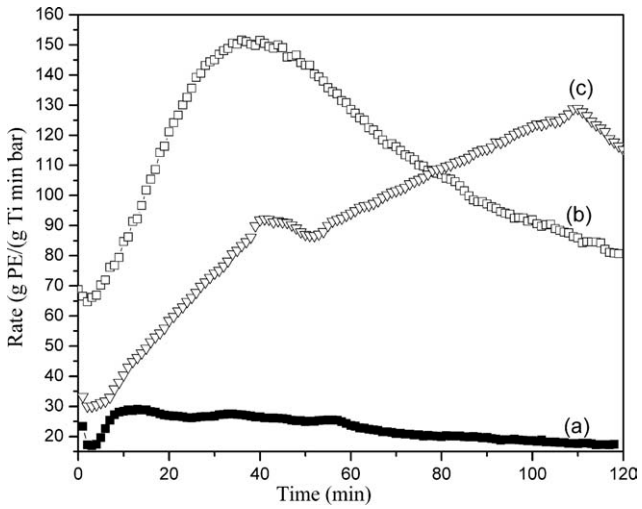


**Figure 5** The activity profiles of catalysts with different PSA contents in ethylene homopolymerization (a) Run 0, (b) Run 2, and (c) Run 7.

activity profiles of three catalysts gradually increased at the initial stage of polymerization and then decayed. SMT performed the lowest activity, although it had the highest titanium content among the three catalysts. This is because that a large amount of ineffective sites (Ti—O) are generated due to the intensive reaction between $TiCl_4$ and 1,4-butanediol. The presence of PSA shell limits the mass transfer of $TiCl_4$ and slows down the reaction between $TiCl_4$ and 1,4-butanediol. Both the titanium content and the amount of the ineffective sites (Ti—O) in the catalysts are reduced in SMPT. Thus, SMPT-1 and SMPT-2 have much higher activity than SMT. On the other hand, increasing PSA content the catalysts take longer time to reach the maximum activity at initial stage. The PSA layer on the composite support can limit the mass transfer of the reactants. As a result, the polymerization initially enters a diffusion-controlled inductive period. As polymerization proceeds, more reactants diffuse inside the whole catalyst particle, and the activity slowly increases until reaching the maximum value. SMPT-2 requires the longest time to achieve the maximum activity due to its highest PSA content. The obvious oscillation in the profile of SMPT-2 is caused by the unstable diffusion of reactants.

The PSA content influences not only the activity profiles but also the polyethylene properties. As displayed in Table III, the weight average MW ($M_w$) of polyethylene produced by SMT is 767,008, whereas the $M_w$ of polyethylene produced by SMPT-1 is 491,470. The presence of PSA dramatically reduces the $M_w$ of the produced polyethylene. Further, the $M_w$ of polyethylene produced by SMPT-2 is 483,006, less than that by SMPT-1. This indicates that the $M_w$ of the produced polyethylene decreases with increasing PSA content in the catalysts. This tendency is confirmed by the result of MFI measurements, also. The polymer MFI was measured as the signature for the MW of polyethylene. The MFI of the polyethylene produced by SMT is undetectable, which means that the MW is too high. However, the MFI of the polyethylene produced by SMPT-1 and SMPT-2 increases to 0.18 and 0.25, respectively. Therefore, it is possible to control the MW of the synthesized polyethylene by adjusting the PSA content in the composite support.

## Effect of hydrogen content on ethylene polymerization by SMPT-1

The effect of hydrogen on the homopolymerization kinetics becomes apparent by comparison of reaction kinetics in the absence and presence of hydrogen (Fig. 6). We observed two distinguishable periods in each profile, containing the increasing stage and gradually decaying stage. The first qualitative conclusion, which can be made from Figure 6, is that the catalyst activity decreases with the growing hydrogen content. Meanwhile, the decay of activity profile was accelerated by the presence of hydrogen. This can be explained by the different diffusion capabilities of hydrogen and ethylene through the PSA layer. More hydrogen than ethylene can pass through the PSA layer to contact the inner active sites. The part inside and outside of the PSA layer is defined as the inner and outer particles, respectively. The hydrogen concentration in the inner particle should be higher than in the outer particle. So, the activity of the inner active sites reduced more than that of the outer active sites. This leads to the faster decay in the activity profile.

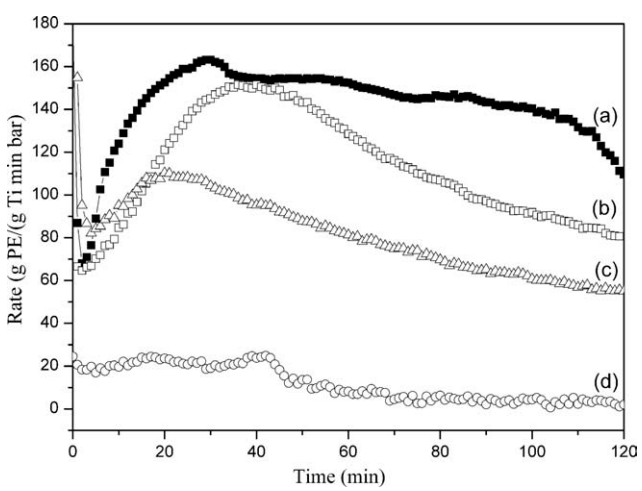


**Figure 6** Hydrogen effect on kinetics of ethylene homopolymerization of SMPT-1 (a) Run 1, (b) Run 2, (c) Run 3, and (d) Run 4.

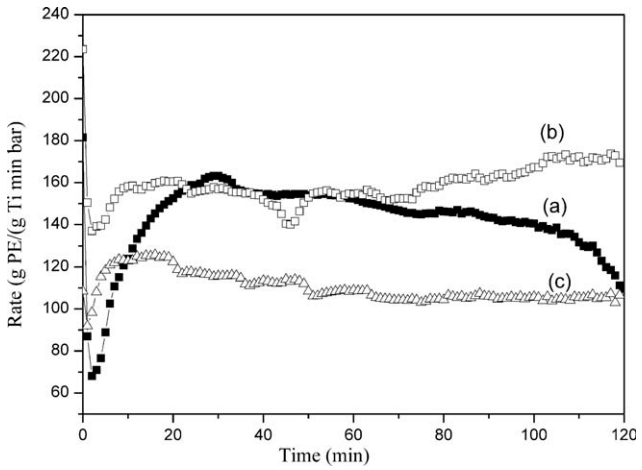


**Figure 7** 1-hexene effects on kinetics of ethylene copolymerization of SMPT-1 (a) Run 1, (b) Run 5, and (c) Run 6.

The hydrogen effect on the MW and MWD of produced polymers is shown in Table III. The MW and MWD of the polyethylene produced by SMPT-1 can be changed from high MW and broad MWD to lower MW and narrower MWD, depending on the hydrogen content. In the absence of hydrogen, a broad MWD ($M_w$ = 741,629, $M_w/M_n$ = 11.6) was observed. Much lower MW and narrower MWD of PE ($M_w$ = 491,470, $M_w/M_n$ = 8.0) was observed at $H_2/C_2H_4$ = 0.5/8.0. The MW of the product significantly decreases with the hydrogen content, demonstrating that hydrogen is effective in chain transfer of SMPT-1. This result is confirmed by the decreasing melting point and increasing MFI of the product in the presence of hydrogen. Furthermore, the $M_w/M_n$ of the produced polyethylene reduced with increasing hydrogen ratio. This is also attributed to the different diffusion capabilities of hydrogen and ethylene through the PSA layer. More hydrogen can pass through the PSA layer, leading to a higher $H_2/C_2H_4$ ratio around the inner active sites. The MW of polyethylene produced by the inner active sites reduced more than that produced by the outer active sites. So, the difference in the MW of polyethylene produced by the inner and outer active sides becomes smaller in the presence of hydrogen, leading to a narrower MWD. Normally, the $M_w/M_n$ of polyethylene produced by commercial Ziegler–Natta catalysts in one reactor is between 4 and 6. When compared with the commercial Ziegler–Natta catalysts, SMPT-1 can produce polyethylene with broader MWD. Different diffusion capabilities and multiple active sites with different propagation, termination, and chain transfer rates[21] formed by loading $TiCl_4$ on the composite support are the reasons for the variation in the MWD of the produced polyethylene.

### Effect of comonomer concentration on ethylene/1-hexene copolymerization by SMPT-1

The effect of comonomer on ethylene polymerization activity and polymer properties was investigated in a series of polymerizations. The activity profiles are shown in Figure 7, from which it can be seen that with a very short polymerization time (10 min), the activity increased in the presence of 1-hexene. Although the productivity of SMPT-1 is improved at a comonomer concentration of 0.109 mol/L, it is reduced at higher concentration (0.218 mol/L) for 120 min polymerization time. This is consistent with the others' conclusions that too high comonomer concentration can reduce the catalysts activity.[40] Besides the activity, the comonomer content strongly affected the time in which the catalysts reach the maximum activity at the initial stage of polymerization. The maximum activity was achieved in 30 min in the absence of 1-hexene. By contrast, the maximum value at the initial stage was observed at 10 and 7 min on the activity profile with 1-hexene at concentration of 0.109 and 0.218 mol/L, respectively. 1-Hexene helped the catalyst to reach the maximum activity in a shorter time. 1-Hexene may enhance the swelling of PSA, leading to reduction of mass-transfer limitation from the PSA shell in copolymerization process. In addition, the decay was slowed down in the activity profiles of copolymerization. This can be explained by stabilizing effect of comonomer on the sites activated by ethylene, and in this way, the deactivation is slowed down.[41]

The GPC spectra of the polymer produced under various 1-hexene concentrations are given in Figure 8. The GPC spectra demonstrate that the polyethylene produced by SMPT-1 change from high MW and broad MWD to low MW and narrow MWD by raising the 1-hexene concentration. Notice that the

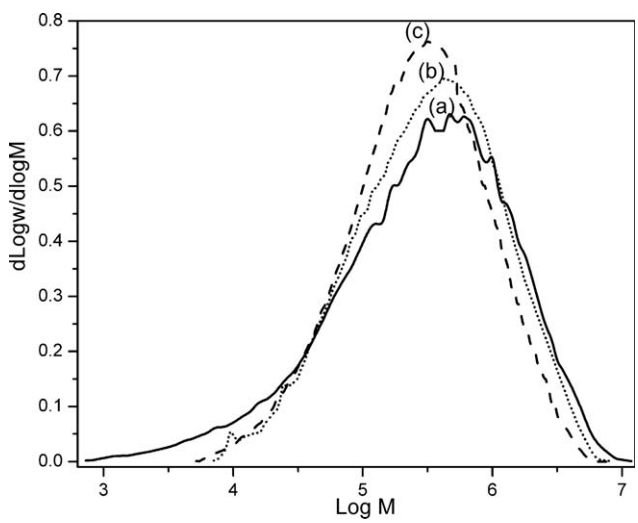


**Figure 8** 1-Hexene effect on the MWD of the produced polymer (a) Run 1, (b) Run 5 and (c) Run 6.

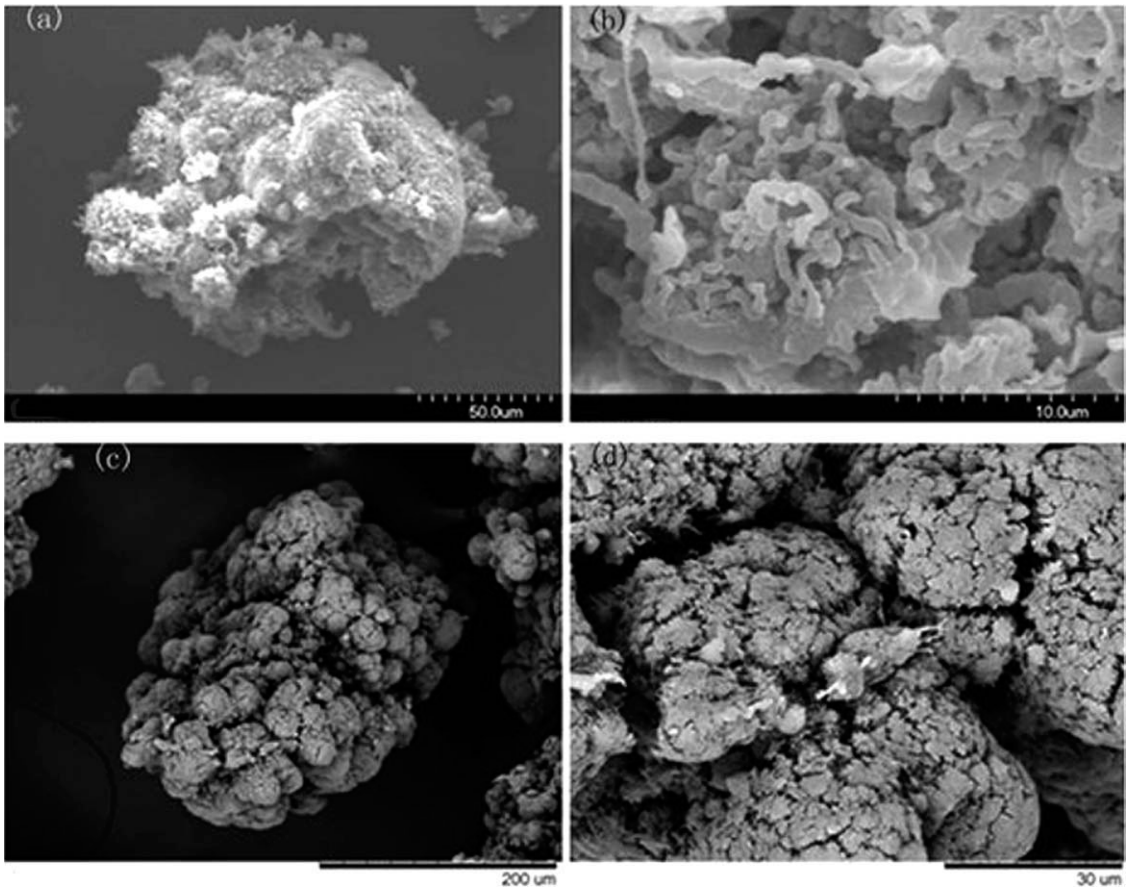


**Figure 9** The SEM images of the polyethylene produced by SMT: (a) and (b), by SMPT (c) and (d).

span of horizontal axis was narrower in the GPC spectrum of copolymer. The component of polyethylene with very low MW (less than 4000) almost diminished in the presence of 1-hexene. More polyethylene with $M_w$ from 35,400 to 320,000 g/mol was produced when the concentration of 1-hexene increased. The $M_w/M_n$ is 11.6 in the absence of comonomer while it decreased to 4.7 at comonomer concentration of 0.109 mol/L. By further increase in comonomer concentration to 0.218 mol/L, the $M_w/M_n$ decreased to 4.1. It is a common point of view that Ziegler–Natta catalyst system has multiple active sites.[42] The presence of *1*-hexene may deactivate the sites, which produce polyethylene with extremely low and high MW. As a result, the polymer synthesized in the presence of 1-hexene has narrower MWD. The melting point and MFI of the produced polymer were also detected. As expected, the produced polymer showed decreasing melting point and growing MFI when the comonomer content increased.

## Morphology of polyethylene

It is well established that the properties and structure of the support together with its fragmentation ability have strong influence on polymerization behavior of the catalyst system.[1,43,44] This was also confirmed by the results of polymerization presented in Table III. To study the morphology of the synthesized polymer particles by SMT and SMPT, SEM photos were taken (Fig. 9). The support morphology as already described was found to be spherical shaped, whereas both polyethylene particles have granular morphology. The polymer produced by SMT seems to be loose and frail at lower magnification 600× in Figure 9(a), and some small debris was also observed. At higher magnification of 5000× [Fig. 9(b)], the polymer granular seems to be porous and constructed from a lot of worm-like polymer. The support of SMT [$SiO_2/MgCl_2{\cdot}x$BD, Fig. 2(c)] was also loose and frail. So, a complete fragmentation of catalyst particles should take place at the beginning of polymerization process when SMT is used. On the other hand, the polymer produced by SMPT is found to be engulfed with spherical primary particles [Fig. 9(c)]. At higher magnification of 2000× [Fig. 9(d)], the particle seems to be tighter and has less porosity. These described differences in the morphology of polymer particles produced by SMT and SMPT indicate that the PSA shell strongly affects the fragmentation behavior of catalyst. The

inner active sites of SMPT-1 are not initially effective due to the limitation of mass-transfer from the PSA layer. Thus, entire particle fragmentation will not occur at the beginning of the polymerization process.[45,46] As polymerization proceeds, layer-by-layer fragmentation of catalyst particles from outside to inside will occur in the ethylene polymerization of SMPT-1.[44] Finally, denser polymer particles with improved bulk density were obtained. The data of bulk density in Table III are confirmed this conclusion. The density of the produced polyethylene by SMT was 0.176 g/cm$^3$ while SMPT produced polyethylene with much higher bulk density, which achieved to 0.325 g/cm $^3$ under the same polymerization condition.

## CONCLUSIONS

The article described the effects of PSA on the performance of a titanium-based Ziegler–Natta catalyst immobilizing on a composite support $SiO_2$/$MgCl_2$·xBD/PSA. The spherical composite support was prepared by precipitation of $MgCl_2$·xBD and PSA on $SiO_2$ step by step. Immobilizing $TiCl_4$ on this composite support with different PSA content resulted in SMPT catalysts with a unique core-mantle-shell structure. $SiO_2$/$MgCl_2$·xBD/$TiCl_4$ (SMT) catalyst without PSA shell was also synthesized for comparison.

The results of catalysts characterization and ethylene polymerization indicated that the PSA layer in the composite support showed different transport capabilities to the reactants. We concluded that PSA had a barrier effect to the diffusion of reactants. Because of the mass transfer limitation of $TiCl_4$, the presence of PSA sharply reduced the titanium content in SMPT. Less ineffective sites were created, leading to higher activity of SMPT in comparison with SMT. Under the same polymerization conditions, the PSA content influenced the activity profiles, including the time for reaching maximum activity and the average activity. Furthermore, SMPT can produce polyethylene with higher MW and broader MWD than the commercial Ziegler–Natta catalysts. This was interpreted by the different diffusion capabilities of reactants and the multiple active sites in SMPT. The barrier effect was also observed in the presence of hydrogen or 1-hexene in the polymerization process. Meanwhile, the incorporation of hydrogen and 1-hexene reduced the MW and narrowed the MWD of polyethylene. The fragmentation of the catalyst and the growth of the polymer particles were also affected by the PSA. Polymerization by the catalyst with PSA shell tended to take place from the exterior of a particle because of limited reactants diffusion. Layer-by-layer fragmentation from outside to inside of particles was supposed to take place in the polymerization of SMPT. In contrast, SMT without PSA fragmented at the entire catalyst particle at the initial stage of polymerization.

All the NMR measurements were carried out in Technische Universität Ilmenau, Germany. They also provided the language help. Thanks for all the help from the group of Prof. Siegfried Stapf.

## References

1. Böhm, L. L. Angew Chem Int Ed Engl 2003, 42, 5010.
2. Kashiwa, N. J Polym Sci Part A: Polym Chem 2004, 42, 1.
3. Malpass, D. B. Introduction to industrial Polyethylene: Properties, Catalysts, and Process; Wiley, 2010; Chapter 3, p 33.
4. McKenna, T. F. L.; Martino, A. D.; Weickert, G.; Soares, J. B. P. Macromol React Eng 2010, 4, 40.
5. Souza, J. L.; Fabri, F.; Buffon, R.; Schuchardt, U. Appl Catal A: Gen 2007, 323, 234.
6. Perin, S. G. M.; Severn, J. R.; Koning, C. E.; Chadwick, J. C. Macromol Chem Phys 2006, 207, 50.
7. Huang, R.; Malizia, F.; Pennini, G.; Koning, C. E.; Chadwick, J. C. Macromol Rapid Commun 2008, 29, 1732.
8. Fukuda, K.; Liu, B.; Nakatani, H.; Nishiyama, I.; Yamahiro, M.; Terano, M. Catal Commun 2003, 4, 657.
9. Pullukat, T. J.; Hoff, R. E. Catal Rev 1999, 41, 389.
10. Wang, J.; Wang, L.; Gao, H.; Wang, W.; Wang, W.; Zhao, Z.; Sun, T.; Feng, L. Polym Int 2006, 55, 299.
11. Vakili, M.; Arabi, H.; Mobarakeh, H. S.; Ghafelebashi, M. J Appl Polym Sci 2010, 118, 2216.
12. Pomogailo, A. D. Polym Sci Ser A 2008, 50, 1204.
13. Gupta, V.; Vinod, C. P.; Kulkarni, G. U.; Lahiri, G. K.; Maity, N.; Bhaduri, S. Curr Sci 2005, 88, 1162.
14. Jericó, S.; Schuchardt, U.; Joekes, I.; Kaminsky, W.; Noll, A. J Mol Catal A: Chem 1995, 99, 167.
15. Sun, L.; Hsu, C. C.; Bacon, D. W. J. J Polym Sci Part A: Polym Chem 1994, 32, 2127.
16. DiMaio, A. J.; Meverden, C. C.; Becker, P. D. U.S. Pat. 6,218,331-B1 ( 2001).
17. Dioos, B. M. L.; Vankelecom, I. F. J.; Jacobs, P. A. Adv Synth Catal 2006, 348, 1413.
18. Roscoe, S. B.; Gong, C.; Frechet, J. M. J.; Walzer, J. F. J Polym Sci Part A: Polym Chem 2000, 38, 2979.
19. Alt, F. P.; Böhm, L. L.; Enderle, H.; Berthold, J. Macromol Symp 2001, 163, 135.
20. Touloupides, V.; Kanellopoulos, V.; Pladis, P.; Kiparissides, C.; Mignon, D.; Van-Grambezen, P. Chem Eng Sci 2010, 65, 3208.
21. Böhm, L. L.; Enderler, H. F.; Fleissner, M. In Catalyst Design for Tailor-Made Polyolefins; Soga, K.; Terano, M., Eds.; Elsevier: Amsterdam, 1994; p 109.
22. Nikolaeva, M. I.; Mikenas, T. B.; Matsko, M. A.; Echevskaya, L. G.; Zakharov, V. A. J Appl Polym Sci 2010, 115, 2432.
23. Guo, Y.; Zhang, X.; Dong, W. J Mol Catal A: Chem 2005, 237, 45.
24. Sun, L.; Hsu, C. C; Bacon, D. W. J Polym Sci Part A: Polym Chem 1994, 32, 2135.
25. Kaur, S.; Singh, G.; Kothari, A. V.; Gupta, V. K. J Polym Sci Part A: Polym Chem 2008, 46, 7299.
26. Liu, C. B.; Tang, T. B.; Huang, B. T. J Polym Sci A: Polym Chem 2001, 39, 2085.
27. Du, L.; Qin, W.; Wang, J.; Yang, Y.; Wu, W.; Jiang, B. Polym Int 2011, 60, 584.
28. Du, L.; Li, W.; Fa, L.; Jiang, B.; Wang, J.; Yang, Y.; Liao, Z. J Appl Polym Sci 2010, 118, 1743.
29. Li, W.; Jiang, B.; Wang, J.; Yang, Y. Polym Int 2011, 60, 676.

30. Jamjah, R.; Zohuri, G. H.; Vaezi, J.; Ahmadjo, S.; Nekomanesh, M.; Pouryari, M. J Appl Polym Sci 2006, 101, 3829.
31. Ye, J.; Huang, H.; Zhang, L.; Wang, J.; Jiang, B.; Yang, Y.; Liao, Z. J Zhejiang Univ (Eng Sci) 2011, 45, 907.
32. Ren, X. H.; Bertmer, M.; Stapf, S.; Demco, D. E.; Blümich, B.; Kern, C.; Jess, A. Appl Catal A: Gen 2002, 228, 39.
33. Keeler, J. Understanding NMR Spectroscopy; Wiely, 2002; Chapter 9, p 42–43.
34. Petry, C. F.; Capeletti, L. B.; Stedile, F. C.; Santos, J. H. Z.; Pozebon, D. Anal Sci 2006, 22, 855.
35. Courivaud, F.; Hansen, E. W.; Karlsson, A.; Kolboe, S.; Stöcker, M. Microporous Mesoporous Mater 2000, 35–36, 327.
36. Dvoyashkin, M.; Khokhlov, A.; Naumov, S.; Valiulin, R. Microporous Mesoporous Mater 2009, 125, 58.
37. Choudhury, R. P.; Schönhoff, M. J Chem Phys 2007, 127, 234702–1.
38. Choudhury, R. P.; Galvosas, P.; Schönhoff, M. J Phys Chem B 2008, 112, 13245.
39. Bernardo, G.; Vesely, D. J Polym Sci 2010, 116, 1348.
40. Smit, M.; Zheng, X.; Brüll, R.; Loos, J.; Chadwicl, J. C.; Koning, C. E. J Polym Sci Part A: Polym Chem 2006, 44, 2883.
41. Xu, Z. G.; Chakravarti, S.; Ray, W. H. J Appl Polym Sci 2010, 80, 81.
42. Matsko, M. A.; Echevskaya, L. G.; Zakharov, V. A.; Nikolaeva, M. I.; Mikenas, T. B.; Vanina, M. P. Macromol Symp 2009, 282, 157.
43. McKenna, T. F.; Soares, J. B. P. Chem Eng Sci 2001, 56, 3931.
44. Chang, M.; Liu, X.; Nelson, P. J.; Munzing, G. R.; Gegan, T. A.; Kissin, Y. V. J Catal 2006, 239, 347.
45. Choi, Y.; Soares, J. B. P. Polymer 2010, 51, 2271.
46. Zheng, X.; Loos, J. Macromol Symp 2006, 236, 249.